Applications of mathematical analysis to tumour acidity modelling

By

Jessica B. McGILLEN, Natasha K. MARTIN, Ian F. ROBEY,

Eamonn A. GAFFNEY, and Philip K. MAINI

Reprinted from

RIMS Kôkyûroku Bessatsu

B31, 2012

RIMS Kôkyûroku Bessatsu
B31 (2012), 31–59

Applications of mathematical analysis to tumour acidity modelling

This paper is dedicated to Professor Yasumasa Nishiura on the occasion of his 60th birthday.

By

Jessica B. McGillen*, Natasha K. Martin**,***, Ian F. Robey†, Eamonn A. Gaffney*, and Philip K. Maini*‡§

Abstract

We propose two mathematical models for acid-mediated tumour invasion, motivated by experimental studies of the safety and efficacy of bicarbonate buffer therapy in mice. We first present a system of coupled nonlinear partial differential equations to describe the effect of buffering therapy on primary and metastatic tumours in tissues of differing density. We then utilise asymptotics to derive an approximation for the minimum invasive wavespeed, taking into account subtleties arising from the problem of high system dimension. Subsequently, we present a system of coupled nonlinear ordinary differential equations to describe systemic tumour and blood buffering through the HCO_3^-/CO_2 buffering system. By finding a uniformly valid analytical approximation to the solution under nonstandard scalings, we obtain predictions for the translational safety and efficacy of bicarbonate therapy in humans. Together these models demonstrate the importance of mathematical analysis in efforts to gain a comprehensive understanding of tumour acidity and invasion.

Received April 18, 2011.
2000 Mathematics Subject Classification(s): 34, 35, 41, 92
Key Words: Tumour acidity, bicarbonate therapy, ordinary differential equations, partial differential equations, asymptotics, separation of timescales

*Centre for Mathematical Biology, Mathematical Institute, University of Oxford, 24-29 St. Giles', Oxford, OX1 3LB, UK.
**Department of Social Medicine, University of Bristol, Canynge Hall, 39 Whatley Road, Bristol, BS8 2PS, UK.
***Department of Global Health and Development, London School of Hygiene and Tropical Medicine, Keppel Street, London, WC1E 7HT, UK.
†Arizona Cancer Center, University of Arizona, Tucson, AZ, 85721, USA.
‡Oxford Centre for Integrative Systems Biology, Department of Biochemistry, University of Oxford, South Parks Road, Oxford, OX1 3QU, UK.
§Corresponding author. E-mail: maini@maths.ox.ac.uk

§ 1. Introduction

We are interested in modelling tumour acidity in the context of the tissue microenvironment. To address questions regarding the safety and efficacy of bicarbonate therapy, a possible new treatment approach that has emerged from experimental studies of tumour acidity in mice, we have derived models comprising systems of coupled nonlinear partial differential equations (PDEs) and coupled nonlinear ordinary differential equations (ODEs). The remainder of this section presents the biological background and general motivation for these models, and Section 2 outlines the specific experimental results and open questions on which they are founded. In Sections 3 and 4 we present the models and carry out asymptotic analyses to gain mathematical, and subsequently biological, insight into the dynamics of each.

§ 1.1. Acid-mediated tumour invasion

In recent years it has become evident that cellular metabolism plays a central role in malignancy [1]: accumulating tumour cells cause a progressive harshening of the local tissue environment, exerting selection pressures and forcing cells to alter their metabolic pathways in order to optimise energy production and continue dividing. This interplay between cell and microenvironment is complex and highly nonlinear with important dynamics at multiple scales.

Of particular interest is the acid-mediated invasion hypothesis [2], which concerns oxygen deprivation in a tissue harbouring a developing tumour: as mutant cells proliferate excessively, the increasingly crowded tissue becomes subject to abnormal perfusion, and thus to hypoxia (local oxygen deprivation), due to inadequate compensation for diffusion-limited transport by leaky, irregular tumour-induced capillary beds. Separation of pre-invasive carcinomas from healthy vasculature by the basement membrane exacerbates this condition. Maintaining ATP production in a hypoxic environment requires adoption of the glycolytic phenotype [3], an alteration in tumour cell metabolism whereby the glycolytic pathway is constitutively upregulated. Acidic by-products of this pathway are toxic to cells, so to survive, tumour cells exhibiting the glycolytic phenotype acquire resistance to the acid they are producing, while normal cells remain susceptible. The acid-mediated invasion hypothesis proposes that a critical stage in the development of an invasive cancer comprises this metabolic shift and resulting selective acidosis.

§ 1.2. The role of mathematical modelling in understanding tumour invasion

Tumour progression is a highly complex, nonlinear, multiscale process, and thus far the intuitive lines of thought that accompany purely experimental approaches have failed to

provide a comprehensive theoretical framework within which to organise and synthesize data [4]. An alternative approach is called for that employs the power of mathematical modelling and analysis to elucidate the core drivers of malignancy in the context of tumour metabolism and the microenvironment. Better understanding possible drivers of malignancy, particularly acid-mediated invasion, may suggest treatments by indicating how best to prevent or delay tumour development.

Gatenby and Gawlinski presented the first continuum mathematical model of acid-mediated invasion [5]: They considered a one-dimensional ray extending out from the centre of an intermediate carcinoma *in situ* exhibiting the glycolytic phenotype, and proposed a system of coupled nonlinear PDEs to describe changes in the densities of healthy and tumour cells and levels of excess extracellular acid. Central to the model was the idea that a fully healthy tissue operating at its carrying capacity would confine a tumour unless diminished by tumour-derived acid. With this model the authors discovered a previously unreported interstitial gap between retreating healthy cells and the advancing tumour front under conditions of high tumour aggressiveness, and subsequently observed gaps in specimens of human squamous cell carcinoma and *in vitro* experiments with rat colon cancer. One therapeutic possibility that has emerged from this modelling rests on the idea that it may be possible to block tumour invasion by applying a buffer to neutralise tumour-derived tissue acidosis and prevent the healthy cell death that opens space for tumour expansion [6]. Our modelling emerges from experiments designed to test the potential of one such therapy, the inexpensive and readily available base bicarbonate. These experiments are detailed in the following section.

§ 2. Experiments to investigate bicarbonate therapy

We have investigated the potential of bicarbonate buffer therapy by orthotopically implanting metastatic MDA-mb-231 adenocarcinomas into the mammary fatpads of 6-week-old female mice with severe combined immunodeficiency (SCID). Beginning six days after tumour inoculation and continuing for the duration of the experiment, the mice were provided with drinking water *ad libitum* containing 200mM bicarbonate ($NaHCO_3$). Control mice were kept under identical conditions with normal drinking water. Effects of $NaHCO_3$ treatment on tumour pH were measured with 31P magnetic resonance spectroscopy (MRS) four weeks after inoculation. Intracellular pH (pHi) was measured with the resonant frequency of inorganic phosphate, while extracellular pH (pHe) was measured with the exogenous pH indicator, 3-aminopropylphosphonate (3-APP). The tumour pHe increased to 7.4 ± 0.06 in the presence of $NaHCO_3$, compared with pH 7.0 ± 0.11 under control conditions. These data also showed that pHi was unaffected; it was 7.00 ± 0.06 and 7.06 ± 0.09 under treated and control conditions, respectively. Surprisingly, we observed an unaltered growth rate of the primary tumour

in the presence of $NaHCO_3$ (Figure 1a).

Following these results in primary tumours, we aimed, in light of the acid-mediated invasion hypothesis, to establish first whether bicarbonate treatment might instead inhibit the formation and growth of metastases, and second whether this inhibition could be sufficient to improve survival. To investigate the former question, control and $NaHCO_3$ treated tumour-bearing mice were euthanized and examined for organ metastases. Tumour xenografts were made from metastatic MDA-mb-231 breast adenocarcinoma cells stably expressing beta-galactosidase (β-gal), and after a 30-day treatment course, the animals were sacrificed and their organs examined for lesions expressing β-gal. Lung lesion diameters were measured and counted in all animals. We found significantly fewer ($p=0.03$) and smaller ($p<0.0001$) metastatic lesions in the $NaHCO_3$ treated group (Figure 1c,d).

To assess survival, female SCID mice bearing green fluorescent protein (GFP) and expressing MDA-mb-231 mammary fatpad xenografts were chronically maintained on 200mM $NaHCO_3$ in drinking water or left untreated. Mice received survival surgery on primary tumours between 35 and 42 days after inoculation, and were euthanized only after they began to exhibit morbidity or obvious lymphatic metastases. Mice maintained on oral bicarbonate survived longer than their untreated counterparts ($p=0.019$, Figure 1b); these data are notable in that the effect of bicarbonate therapy was greater than in previous experiments, yet the median time until sacrifice was significantly longer, indicating that selective tumour alkalinization by chronic oral ingestion of $NaHCO_3$ is sufficient to significantly improve survival status in tumour-bearing mice.

§ 2.1. Open biological questions

Two main biological questions emerge from these experimental findings. First, why does bicarbonate therapy reduce metastatic but not primary tumour growth in mice? Second, what is the translational safety and efficacy of bicarbonate therapy in humans? To explore these questions and indicate further experimental directions, we develop and analyse two extensions of the Gatenby and Gawlinski model [5], described in Sections 3 and 4.

§ 3. Efficacy of bicarbonate therapy in primary and metastatic tumours

§ 3.1. A system of coupled nonlinear partial differential equations

Here we address the first of our experimentally-motivated questions; that is, why bicarbonate-mediated alkalinisation reduces the number and size of metastatic but not primary tumours. We postulate that in our experiments, the primary tumours grew in relatively low-density tissues (the mammary fat pads) and thus had spatial freedom to expand

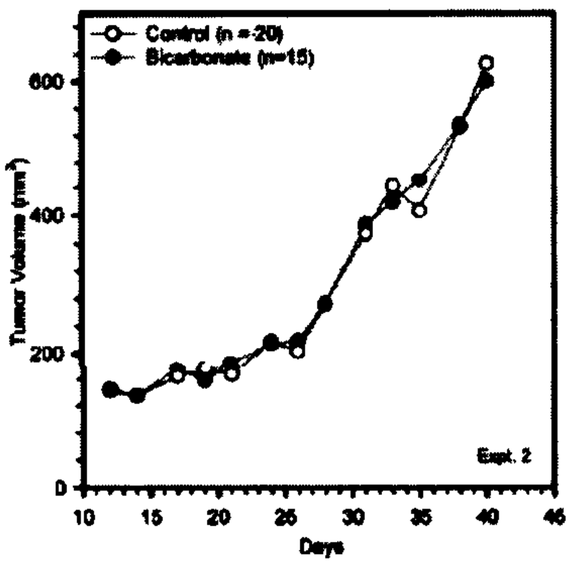

(a)

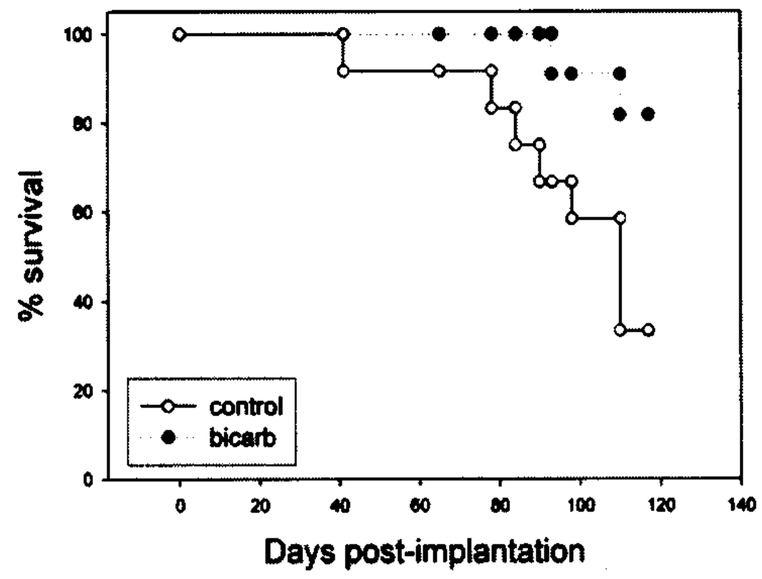

(b)

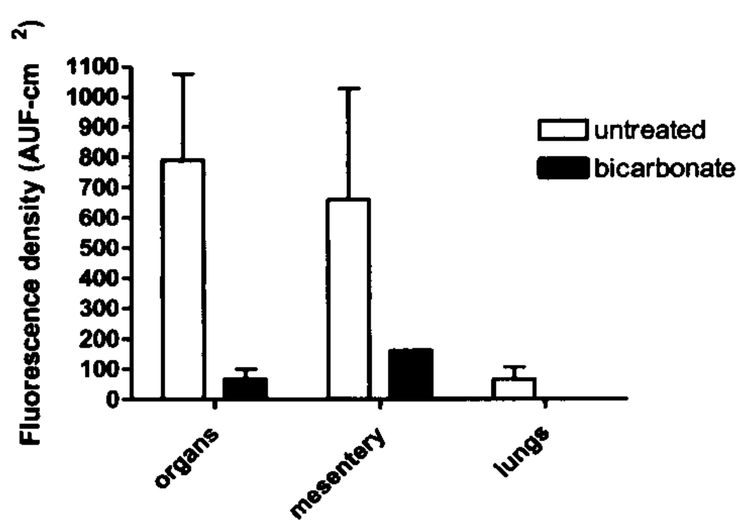

(c)

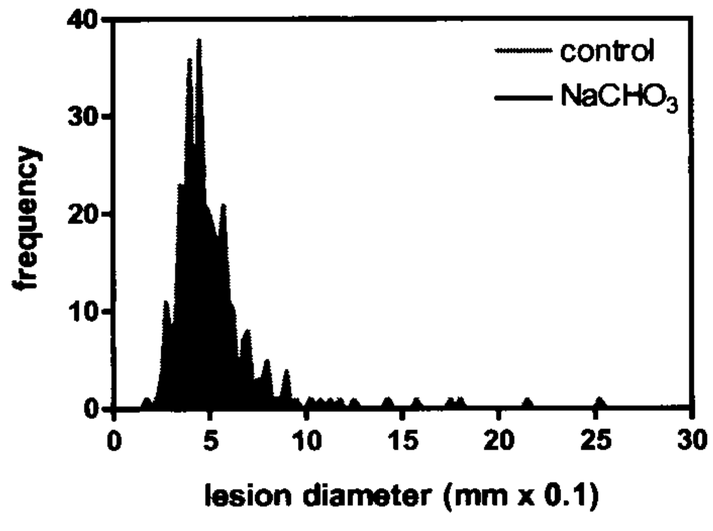

(d)

Figure 1: a) Average primary tumour growth over 40 days with control and bicarbonate treated mice. Note the identical primary tumour growth curves in each group. b) Kaplan-Meier survival curve in cohorts of control and $NaHCO_3$ treated mice whose primary tumours were surgically removed after approximately 30 days of growth. Log-rank analyses showed that these two populations were significantly different (p=0.019). c) Metastatic mean flourescence pixel densities (flourescence intensities $\times$ area) for visceral organs, mesentary, and lungs (bars show standard error). d) Histogram of lesion frequency by diameter in $NaHCO_3$ treated group is smaller than in untreated control group after 30 days. Figures reproduced from reference [7] in accordance with AACR copyright and permission policies.

even when actively buffered, while at least some of the metastases grew in high-density tissues, such as the liver and spleen, so were more dependent on acid-mediated invasion. To test this idea, we extend the system in [5] to include additional buffering (implicitly through oral bicarbonate administration) and a dependence of invasive ability on tissue

density. The extended, nondimensionalised model is as follows, with η_1 representing normal cell density, η_2 the tumour cell density, and Λ the density of excess extracellular H^+ ions:

$$\frac{\partial \eta_1}{\partial \tau} = \eta_1(1-\eta_1) - \gamma_1 \Lambda \eta_1 \tag{3.1}$$

$$\frac{\partial \eta_2}{\partial \tau} = \delta_2 \eta_2(1-\eta_2) + \nabla_\xi \cdot \left[\alpha_2\left(1 - \frac{\eta_1}{1+K_*^{tis}}\right)\nabla_\xi \eta_2\right] \tag{3.2}$$

$$\frac{\partial \Lambda}{\partial \tau} = \delta_3(\eta_2 - \Lambda) - \gamma_3 \Lambda + \nabla_\xi^2 \Lambda, \tag{3.3}$$

where α_2, γ_1, γ_3, δ_2, and δ_3 are positive constants. The system is solved with Neumann (no-flux) boundary conditions at $\xi = 0$ (representing the tumour centre) and fixed boundary conditions $\eta_1 = 1$, $\eta_2 = 0$, and $\Lambda_2 = 0$ at the right-hand boundary representing the tumour-free state. Initial conditions for the cell populations are semi-compact step functions, with the following transitions at the same spatial location: the tumour population from 1 to 0 and the normal tissue population from 0 to 1. The initial acid concentration is zero across the domain.

As in [5], the nondimensional parameter γ_1 is proportional to the tumour acid production rate, and inversely proportional to the normal cell sensitivity to acid. Hence, we refer to this parameter as the 'aggression' parameter, where high γ_1 indicates either a high amount of acid production or high normal cell sensitivity to acid. Our additions to the model in [5] are captured in two terms in Equations (3.1)-(3.3). First, a loss term ($\gamma_3\Lambda$) is added to represent bicarbonate-mediated proton buffering, proportional to the acid level. Second, tissue density-dependent invasive ability is incorporated via inclusion in the diffusion term of the factor K_*^{tis}, where $tis = p$ for primary tumours and $tis = m$ for metastatic tumours in different tissues. Tumours in dense tissues have a low K_*^{tis}, indicating low freedom of motility, while tumours in looser, acellular tissues have a high K_*^{tis}, indicating greater freedom of movement. A mathematical analysis of this system now enables us to obtain an explicit description of how invasiveness changes as a function of the model parameters, namely tissue density and buffering treatment.

§ 3.2. A travelling wave analysis via matched asymptotic expansion

Numerical simulations (not shown) indicate that tumour density profiles of constant shape arise after the decay of transients and appear to travel at a constant wavespeed. The invasive tumour waves exhibit behaviour similar to the well-studied Fisher-Kolmogorov equation, which is known to evolve to a minimal wavespeed given compact or semi-compact initial conditions. The Fisher-Kolmogorov system has only one species (and therefore is amenable to phase plane analysis), while the existence of an analagous minimal wavespeed for our three-species system remains an open question as the three

species give rise to a five-dimensional phase space on which a Fisher-Kolmogorov analysis is invalid; however, we use asymptotics to reduce our system to two ODEs and thus conjecture the large-time behaviour of the full system. Noting that chemical diffusion of excess acid is much faster than density-dependent diffusion of tumour cells gives us the ratio between the two as a small parameter, denoted α_2 in Equation (3.2), to be exploited for these asymptotics. The analytical procedure follows [8] in which a similar analysis was carried out on the original Gatenby and Gawlinski system [5]. Our analysis differs nontrivially from theirs in two important ways; first, we have altered the tumour diffusion term in Equation (3.2), and second, we have included an additional source of acid loss due to buffering in Equation (3.3).

Transforming our system into travelling wave coordinates via the substitutions $\eta_1 = u(z)$, $\eta_2 = v(z)$, and $\Lambda = w(z)$ into Equations (3.1)-(3.3) where $z = \xi - ct$ and c is the constant wavespeed, yields the system

$$-cu' = u(1-u) - \gamma_1 uw \tag{3.4}$$

$$-cv' = \delta_2 v(1-v) + \alpha_2\left[\left(1 - \frac{u}{1+K_*^{tis}}\right)v'' - \frac{1}{1+K_*^{tis}}u'v'\right] \tag{3.5}$$

$$-cw' = \delta_3(v-w) - \gamma_3 w + w'', \tag{3.6}$$

with $'$ denoting differentiation with respect to z. This transformation reveals the presence of a boundary layer; that is, a narrow inner region unfolds in which the solution and its derivatives are changing rapidly, in contrast to the outer region in which they change only slowly (as seen in Figure 2).

We first find the leading-order contribution to our solution in the outer region, taking into account the boundary conditions, then rescale within the inner region to find a leading-order approximation to the inner solution. Lastly, we match these solutions across the regions of overlap to obtain uniform approximate solutions for all species as explicit functions of the model parameters, and from these extract the constant (assumed minimum) tumour wavespeed.

Four equilibrium points are associated with Equations (3.4)-(3.6):

- $(\tilde{u_1}, \tilde{v_1}, \tilde{w_1}) = (0,0,0)$, a trivial, linearly unstable state with no tissue or excess acid;
- $(\tilde{u_2}, \tilde{v_2}, \tilde{w_2}) = (1,0,0)$, a linearly unstable healthy state with normal tissue at carrying capacity and no tumour or excess acid;
- $(\tilde{u_3}, \tilde{v_3}, \tilde{w_3}) = (1 - \frac{\gamma_1\delta_3}{\delta_3+\gamma_3}, 1, \frac{\delta_3}{\delta_3+\gamma_3})$, a coexistent state with tumour tissue at carrying capacity and diminished normal tissue. This state is biologically realistic for $1 - \frac{\gamma_1\delta_3}{\delta_3+\gamma_3} > 0$ and in that case is linearly stable;
- $(\tilde{u_4}, \tilde{v_4}, \tilde{w_4}) = (0, 1, \frac{\delta_3}{\delta_3+\gamma_3})$, an invaded state with tumour tissue at carrying capacity and no remaining normal tissue, linearly stable if $\gamma_1 > \frac{\delta_3+\gamma_3}{\delta_3}$ and unstable otherwise.

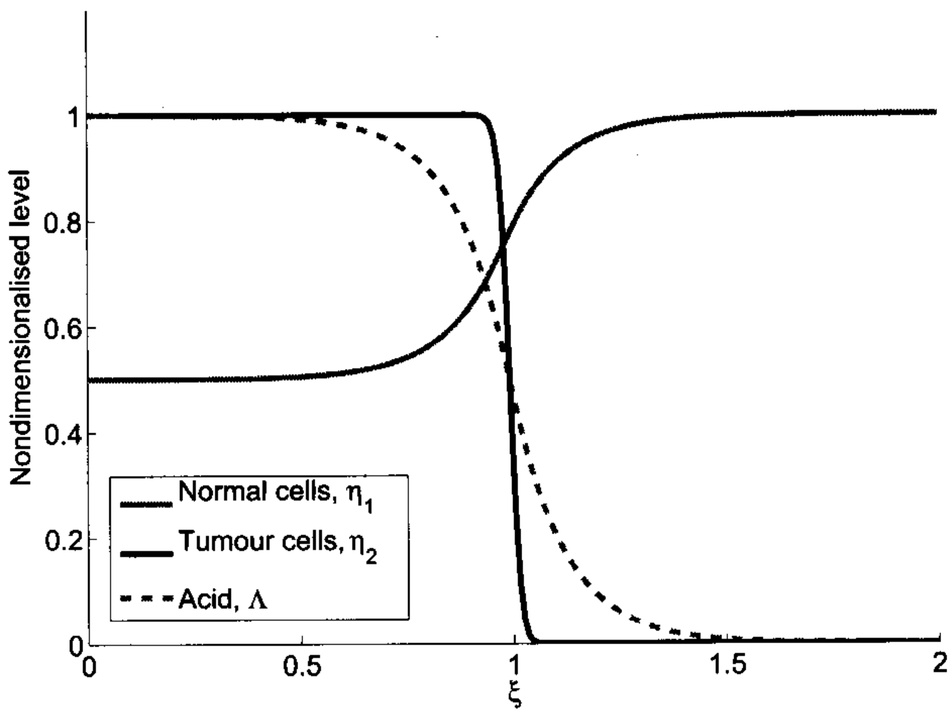

Figure 2: Late-time numerical simulation of Equations (3.1)-(3.3) showing the tumour, normal, and acid travelling waves, where $\gamma_1 = 0.5$, $\delta_2 = 1$, $\alpha_2 = 4 \times 10^{-5}$, $\delta_3 = 70$, $K_* = 0$, and $\gamma_3 = 0$. The system is solved with boundary and initial conditions as described in the text.

We denote the solution to Equations (3.4)-(3.6) by $u = u(z, \alpha_2)$, $v = v(z, \alpha_2)$, and $w = w(z, \alpha_2)$. The travelling wave boundary conditions are then $u(\infty, \alpha_2) = 1$, $v(\infty, \alpha_2) = 0$, $w(\infty, \alpha_2) = 0$, and

$$v(-\infty, \alpha_2) = 1 \tag{3.7}$$

$$w(-\infty, \alpha_2) = \frac{\delta_3}{\delta_3 + \gamma_3} \tag{3.8}$$

$$u(-\infty, \alpha_2) = \begin{cases} 1 - \dfrac{\gamma_1 \delta_3}{\delta_3 + \gamma_3} & \text{if } 0 < \gamma_1 < \dfrac{\delta_3 + \gamma_3}{\delta_3}, \\ 0 & \text{if } \dfrac{\delta_3 + \gamma_3}{\delta_3} \leq \gamma_1. \end{cases} \tag{3.9}$$

We note that, strictly, the healthy steady state should be stable initially, then driven unstable by the forming invasive tumour; however, our modelling assumes the normal steady state has already been destabilised. By doing this we neglect regulatory biological features, such as immunosurveillence, for the purpose of looking beyond very early tumour development to focus on the dynamics of invasion.

Splitting the constant wavespeed into fast and slow components by writing $z = \xi - \epsilon c_0 t$ with $c = c_0\sqrt{\alpha_2}$ and $\alpha_2 = \epsilon^2 << 1$, such that ϵ becomes our small parameter, and scaling $c_0 \sim O(1)$ because we are interested in the invasive waves driven by tumour diffusion dynamics (and we note here that all parameters are $O(1)$ or larger except α_2

which is $O(10^{-5})$), we have

$$-\epsilon c_0 u' = u(1-u) - \gamma_1 uw \tag{3.10}$$

$$-\epsilon c_0 v' = \delta_2 v(1-v) + \epsilon^2 \left[\left(1 - \frac{u}{1+K_*^{tis}} \right) v'' - \frac{1}{1+K_*^{tis}} u'v' \right] \tag{3.11}$$

$$-\epsilon c_0 w' = \delta_3(v-w) - \gamma_3 w + w'', \tag{3.12}$$

Setting $\epsilon = 0$, the leading contributions to the outer solutions satisfy

$$0 = u(1-u) - \gamma_1 uw \tag{3.13}$$

$$0 = \delta_2 v(1-v) \tag{3.14}$$

$$0 = \delta_3(v-w) - \gamma_3 w + w''. \tag{3.15}$$

Rescaling with $z = \epsilon\zeta$ in the inner region, we see that the leading order of the inner solution satisfies

$$-c_0 \dot{u} = u(1-u) - \gamma_1 uw \tag{3.16}$$

$$-c_0 \dot{v} = \delta_2 v(1-v) + \left[\left(1 - \frac{u}{1+K_*^{tis}} \right) \ddot{v} - \frac{1}{1+K_*^{tis}} \dot{u}\dot{v} \right] \tag{3.17}$$

$$\ddot{w} = 0. \tag{3.18}$$

with $\dot{}$ denoting differentiation with respect to ζ.

Further, we define the leading order contribution to the outer solution by the following, where $\alpha_2 = 0$:

$$u_{out}(z) = u(z;0), \quad v_{out}(z) = v(z;0), \quad w_{out} = w(z;0). \tag{3.19}$$

Similarly, the leading order inner solution is

$$U_{in}(\zeta) = U(\zeta;0), \quad V_{in}(\zeta) = V(\zeta;0), \quad W_{in}(\zeta) = W(\zeta;0). \tag{3.20}$$

We now exploit these regions to derive uniform approximations for excess acid (w), healthy density (u), and finally the (assumed minimum) travelling wavespeed of the tumour density (v).

We begin with the uniform approximation for excess acid (w). From Equations (3.13)-(3.15) and noting the boundary conditions, we see that

$$v_{out}(z) = \begin{cases} 1 & \text{if } z < 0, \\ 0 & \text{if } z > 0. \end{cases} \tag{3.21}$$

Substituting this into Equation (3.15) we find

$$w'' + \delta_3\left(1 - w - \frac{\gamma_3}{\delta_3} w\right) = 0 \quad \text{if } z < 0, \tag{3.22}$$

$$w'' - (\delta_3 + \gamma_3) w = 0 \quad \text{if } z > 0. \tag{3.23}$$

In the $z < 0$ case, we have

$$w_{out}(z) = \frac{\delta_3(1 - Be^{\sqrt{\delta_3+\gamma_3}z})}{\delta_3 + \gamma_3}, \tag{3.24}$$

where B is a constant. In the $z > 0$ case, we have

$$w_{out}(z) = Ae^{-\sqrt{\delta_3+\gamma_3}z}, \tag{3.25}$$

where A is a constant.

Looking at the inner solution, we have $\ddot{W}_{in}(\zeta) = 0$ and thus $W_{in}(\zeta) = w_0 + \zeta w_1$. We know this solution is bounded as $\zeta \to \infty$; consequently, W_{in} must be constant (i.e. $w_1 = 0$) and the outer solutions and their derivatives must match each other across the inner region (and take on the value of the constant inner solution). Carrying out this matching across $z = 0$ yields $B = 1/2$ and $A = \delta_3/2(\delta_3 + \gamma_3)$, and accordingly we find

$$W_{in}(\zeta) = \frac{\delta_3}{2(\delta_3 + \gamma_3)}. \tag{3.26}$$

Therefore, the uniform solution for the excess acid profile is

$$w_{unif}(z; \alpha_2) = w_{out}(z) + W_{in}(\frac{z}{\sqrt{\alpha_2}}) - w_{overlap}$$

$$= \begin{cases} \frac{\delta_3}{2(\delta_3 + \gamma_3)} e^{-\sqrt{\delta_3+\gamma_3}z} & \text{if } z > 0, \\ \frac{\delta_3}{\delta_3 + \gamma_3}(1 - \frac{1}{2}e^{\sqrt{\delta_3+\gamma_3}z}) & \text{if } z < 0. \end{cases} \tag{3.27}$$

We now use Equation (3.27) to find an approximation for healthy cell density (u). It is evident that Equation (3.10) is a Bernoulli equation for u:

$$\sqrt{\alpha_2}c_0 u' = \gamma_1 uw - u(1 - u). \tag{3.28}$$

Therefore, we have the solution

$$u(z, \alpha_2) = \begin{cases} \frac{\sqrt{\alpha_2}c_0 e^{\Phi_-(z)/\sqrt{\alpha_2}}}{\int_z^0 e^{\Phi_-(s)/\sqrt{\alpha_2}}ds + \int_0^\infty e^{\Phi_+(s)\sqrt{\alpha_2}}ds} & \text{if } z < 0, \\ \frac{\sqrt{\alpha_2}c_0 e^{\Phi_+(z)\sqrt{\alpha_2}}}{\int_z^\infty e^{\Phi_+(s)\sqrt{\alpha_2}}ds} & \text{if } z > 0, \end{cases} \tag{3.29}$$

with

$$\Phi_-(z) = \frac{1}{c_0}\left[\frac{\gamma_1\delta_3}{2(\delta_3 + \gamma_3)^{3/2}}\left(1 - e^{\sqrt{\delta_3+\gamma_3}z}\right) - z\left(1 - \frac{\gamma_1\delta_3}{\delta_3 + \gamma_3}\right)\right] \tag{3.30}$$

$$\Phi_+(z) = \frac{1}{c_0}\left[\frac{\gamma_1\delta_3}{2(\delta_3 + \gamma_3)^{3/2}}\left(1 - e^{-\sqrt{\delta_3+\gamma_3}z}\right) - z\right]. \tag{3.31}$$

With these definitions of Φ_+ and Φ_- we calculate the following properties which will be used later in the wavespeed derivation to put bounds on functions:

$$\Phi_-(0) = 0 \tag{3.32}$$

$$\Phi_-'(z) = \frac{1}{c_0}\left[\left(\frac{\gamma_1\delta_3}{\delta_3+\gamma_3} - 1\right) - \frac{\gamma_1\delta_3}{2(\delta_3+\gamma_3)}e^{\sqrt{\delta_3+\gamma_3}z}\right] \tag{3.33}$$

$$\Phi_-''(z) = -\frac{\gamma_1\delta_3}{2c_0(\delta_3+\gamma_3)^{1/2}}e^{\sqrt{\delta_3+\gamma_3}z} \tag{3.34}$$

$$\Phi_+(0) = 0 \tag{3.35}$$

$$\Phi_+'(z) = \frac{1}{c_0}\left[\frac{\gamma_1\delta_3}{2(\delta_3+\gamma_3)}e^{-\sqrt{\delta_3+\gamma_3}z} - 1\right] \tag{3.36}$$

$$\Phi_+''(z) = -\frac{\gamma_1\delta_3}{2c_0(\delta_3+\gamma_3)^{1/2}}e^{-\sqrt{\delta_3+\gamma_3}z}. \tag{3.37}$$

Furthermore, if we define

$$z_- = \frac{1}{\sqrt{\delta_3+\gamma_3}}\log\left(2 - \frac{2(\delta_3+\gamma_3)}{\gamma_1\delta_3}\right) < 0 \quad \text{if} \quad \frac{\delta_3+\gamma_3}{\delta_3} < \gamma_1 < \frac{2(\delta_3+\gamma_3)}{\delta_3} \tag{3.38}$$

$$z_+ = \frac{1}{\sqrt{\delta_3+\gamma_3}}\log\left(\frac{\gamma_1\delta_3}{2(\gamma_3+\delta_3)}\right) > 0 \quad \text{if} \quad \frac{2(\delta_3+\gamma_3)}{\delta_3} < \gamma_1 \tag{3.39}$$

then $\Phi_-(z_-) > 0$, $\Phi_-'(z_-) = 0$, $\Phi_-''(z_-) < 0$, $\Phi_+(z_+) > 0$, $\Phi_+'(z_+) = 0$, and $\Phi_+''(z_+) < 0$. An explicit solution for u must be derived in separate cases, which we now examine.

Case A: $0 < \gamma_1 < \frac{\delta_3+\gamma_3}{\delta_3}$
If $z > 0$, then for any $z < s < \infty$ we have

$$\Phi_+'(s) = \frac{1}{c_0}\left[\frac{\gamma_1\delta_3}{2(\delta_3+\gamma_3)}e^{-\sqrt{\delta_3+\gamma_3}s} - 1\right] < \frac{1}{c_0}\left[\frac{\gamma_1\delta_3}{2(\delta_3+\gamma_3)} - 1\right] < 0. \tag{3.40}$$

Using asymptotic expansions of general Laplace integrals at leading order, and invoking the above monotonicity of Φ_+, we have

$$\int_z^\infty e^{\Phi_+(s)/\sqrt{\alpha_2}}ds = -\frac{\sqrt{\alpha_2}e^{\Phi_+(z)/\sqrt{\alpha_2}}}{\Phi_+'(z)}(1+O(\sqrt{\alpha_2})), z > 0 \tag{3.41}$$

so that the leading order approximation to our solution for u from Equation (3.29) becomes, for $z > 0$,

$$\begin{aligned} u(z,\alpha_2) &\approxeq \frac{\sqrt{\alpha_2}c_0e^{\Phi_+(z)/\sqrt{\alpha_2}}}{\int_z^\infty e^{\Phi_+(s)/\sqrt{\alpha_2}}ds} = -\frac{\sqrt{\alpha_2}c_0e^{\Phi_+(z)/\sqrt{\alpha_2}}}{\sqrt{\alpha_2}e^{\Phi_+(z)/\sqrt{\alpha_2}}}\Phi_+'(z) = -c_0\Phi_+'(z) \\ &= 1 - \frac{\gamma_1\delta_3}{2(\delta_3+\gamma_3)}e^{-\sqrt{\delta_3+\gamma_3}z} \quad \text{when } z > 0. \end{aligned} \tag{3.42}$$

If $z < 0$, then for any $0 \leq s < \infty$, as before,

$$\Phi_+'(s) = \frac{1}{c_0}\left[\frac{\gamma_1\delta_3}{2(\delta_3+\gamma_3)}e^{-\sqrt{\delta_3+\gamma_3}s} - 1\right] < \frac{1}{c_0}\left[\frac{\gamma_1\delta_3}{2(\delta_3+\gamma_3)} - 1\right] < 0. \tag{3.43}$$

From Laplace's method,

$$\int_0^\infty e^{\Phi_+(s)/\sqrt{\alpha_2}}ds \cong -\frac{\sqrt{\alpha_2}e^{\Phi_+(0)/\sqrt{\alpha_2}}}{\Phi_+'(0)} = \frac{2c_0\sqrt{\alpha_2}(\delta_3+\gamma_3)}{2(\delta_3+\gamma_3)-\gamma_1\delta_3}. \tag{3.44}$$

For any $z \leq s < 0$,

$$\Phi_-'(s) = \frac{1}{c_0}\left[\left(\frac{\gamma_1\delta_3}{\delta_3+\gamma_3}\right) - \frac{\gamma_1\delta_3}{2(\delta_3+\gamma_3)}e^{\sqrt{\delta_3+\gamma_3}s}\right] \leq \frac{1}{c_0}\left(\frac{\gamma_1\delta_3}{2\delta_3+\gamma_3} - 1\right) < 0, \tag{3.45}$$

so that Lapace's method gives

$$\int_z^0 e^{\Phi_-(s)/\sqrt{\alpha_2}}ds \cong -\frac{\sqrt{\alpha_2}e^{\Phi_-(z)/\sqrt{\alpha_2}}}{\Phi_-'(z)} \quad (z<0). \tag{3.46}$$

Hence,

$$\begin{aligned}\int_z^0 e^{\Phi_-(s)/\sqrt{\alpha_2}}ds + \int_0^\infty e^{\Phi_+(s)/\sqrt{\alpha_2}}ds &\cong -\frac{\sqrt{\alpha_2}e^{\Phi_-(z)/\sqrt{\alpha_2}}}{\Phi_-'(z)} + \frac{2c_0\sqrt{\alpha_2}(\delta_3+\gamma_3)}{2(\delta_3+\gamma_3)-\gamma_1\delta_3} \\ &\cong -\frac{\sqrt{\alpha_2}e^{\Phi_-(z)/\sqrt{\alpha_2}}}{\Phi_-'(z)} \quad (z<0)\end{aligned} \tag{3.47}$$

since $\Phi_-(z) > 0$ for $z < 0$ and $0 < \gamma_1 < \frac{\delta_3+\gamma_3}{\delta_3}$. From Equation (3.29) it follows that the leading order approximation for u is

$$u(z;\alpha_2) \cong -c_0\Phi_-'(z) = 1 - \frac{\gamma_1\delta_3}{\delta_3+\gamma_3} + \frac{\gamma_1\delta_3}{2(\delta_3+\gamma_3)}e^{\sqrt{\delta_3+\gamma_3}z} \quad \text{when } z<0. \tag{3.48}$$

In summary, for the outer region, when $0 < \gamma_1 < \frac{\delta_3+\gamma_3}{\delta_3}$ the leading order approximation for u with respect to $\sqrt{\alpha_2}$ is

$$u(z;\alpha_2) = \begin{cases} 1 - \dfrac{\gamma_1\delta_3}{\delta_3+\gamma_3} + \dfrac{\gamma_1\delta_3}{2(\delta_3+\gamma_3)}e^{\sqrt{\delta_3+\gamma_3}z} & \text{if } z<0, \\ 1 - \dfrac{\gamma_1\delta_3}{2(\delta_3+\gamma_3)}e^{-\sqrt{\delta_3+\gamma_3}z} & \text{if } z>0. \end{cases} \tag{3.49}$$

To assess the presence or absence of an interstitial gap, and thereby determine how our system relates back to the original Gatenby and Gawlinski system [5], we expand u in the inner variables. Letting $z = \sqrt{\alpha_2}\zeta$, we have, from Equation (3.29),

$$U(\zeta;\alpha_2) = u(\sqrt{\alpha_2}\zeta,\alpha_2) \cong \begin{cases} 1 - \dfrac{\gamma_1\delta_3}{\delta_3+\gamma_3} + \dfrac{\gamma_1\delta_3}{2(\delta_3+\gamma_3)}e^{\sqrt{\delta_3+\gamma_3}\sqrt{\alpha_2}\zeta} & \text{if } \zeta<0, \\ 1 - \dfrac{\gamma_1\delta_3}{2(\delta_3+\gamma_3)}e^{-\sqrt{\delta_3+\gamma_3}\sqrt{\alpha_2}\zeta} & \text{if } \zeta>0. \end{cases} \tag{3.50}$$

Setting $\alpha_2 = 0$ gives the leading order approximation

$$U_{in}(\zeta) = 1 - \frac{\gamma_1\delta_3}{2(\delta_3+\gamma_3)} > 0 \quad \text{for any } \zeta \text{ in } \mathbb{R}, \tag{3.51}$$

which matches with the leading order outer solution, and indicates that for $0 < \gamma_1 < \frac{\delta_3+\gamma_3}{\delta_3}$ there is no interstitial gap as the normal tissue approximation is non-zero.

Case B: $\dfrac{\delta_3+\gamma_3}{\delta_3} < \gamma_1 < \dfrac{2(\delta_3+\gamma_3)}{\delta_3}$

If $z > 0$, then the analysis is as in Case A; thus, at leading order,

$$u(z,\alpha_2) = 1 - \frac{\gamma_1\delta_3}{2(\delta_3+\gamma_3)} e^{-\sqrt{\delta_3+\gamma_3}z} \quad \text{for} \quad z > 0 \tag{3.52}$$

and

$$\int_z^\infty e^{\Phi_+(s)/\sqrt{\alpha_2}}ds \approxeq -\frac{\sqrt{\alpha_2}e^{\Phi_+(z)/\sqrt{\alpha_2}}}{\Phi_+'(z)}. \tag{3.53}$$

If $z_- < z < 0$, then for any $z \le s < 0$ we have $z_- < s$ and

$$\begin{aligned}\Phi_-'(s) &= \frac{1}{c_0}\left[\left(\frac{\gamma_1\delta_3}{\delta_3+\gamma_3} - 1\right) - \frac{\gamma_1\delta_3}{2(\delta_3+\gamma_3)} e^{\sqrt{\delta_3+\gamma_3}s}\right] \\ &= \Phi_-'(z_-) + \frac{\gamma_1\delta_3}{2(\delta_3+\gamma_3)}\left[e^{\sqrt{\delta_3+\gamma_3}}z_- - e^{\sqrt{\delta_3+\gamma_3}s}\right] < 0,\end{aligned} \tag{3.54}$$

because $\Phi_-'(z_-) = 0$. Also, as before,

$$\int_z^0 e^{\Phi_-(s)/\sqrt{\alpha_2}}ds + \int_0^\infty e^{\Phi_+(s)/\sqrt{\alpha_2}}ds \approxeq -\frac{\sqrt{\alpha_2}e^{\Phi_-(z)/\sqrt{\alpha_2}}}{\Phi_-'(z)} \tag{3.55}$$

because $\Phi_+(0) > \Phi_+(z)$ for $z > 0$ and $\Phi_-(z) > \Phi_-(s)$ for $z_- < z \le s < 0$. Hence,

$$u(z;\alpha_2) \approxeq -c_0\Phi_-'(z) = 1 - \frac{\gamma_1\delta_3}{\delta_3+\gamma_3} + \frac{\gamma_1\delta_3}{2(\delta_3+\gamma_3)} e^{\sqrt{\delta_3+\gamma_3}z} \quad \text{for } z_- < z < 0. \tag{3.56}$$

If $z < 0$ and $z < z_-$, then using asymptotic expansions of general Laplace integrals at leading order and given that $\Phi_-'(z_-) = 0$ and $\Phi_-''(z_-) < 0$,

$$\int_z^0 e^{\Phi_-(s)/\sqrt{\alpha_2}}ds \approxeq \frac{\sqrt{2\pi}\alpha_2^{1/4}e^{\Phi_-(z_-)/\sqrt{\alpha_2}}}{\sqrt{-\Phi_-''(z_-)}} = \frac{\sqrt{2\pi}\alpha_2^{1/4}e^{\Phi_-(z_-)/\sqrt{\alpha_2}}}{\sqrt{\dfrac{\gamma_1\delta_3}{c_0(\delta_3+\gamma_3)^{1/2}}\left(1 - \dfrac{\delta_3+\gamma_3}{\gamma_1\delta_3}\right)}} \tag{3.57}$$

and since $\Phi_-(z_-)$ is positive and greater than $O(\sqrt{\alpha_2})$, and $\Phi_-(z_-)$ is independent of

α_2,

$$\int_z^0 e^{\Phi_-(s)/\sqrt{\alpha_2}}ds + \int_0^\infty e^{\Phi_+(s)/\sqrt{\alpha_2}}ds \approxeq \frac{\sqrt{2\pi}\alpha_2^{1/4}e^{\Phi_-(z_-)/\sqrt{\alpha_2}}}{\sqrt{\frac{\gamma_1\delta_3}{c_0(\delta_3+\gamma_3)^{1/2}}\left(1-\frac{\delta_3+\gamma_3}{\gamma_1\delta_3}\right)}} + \frac{2c_0\sqrt{\alpha_2}(\delta_3+\gamma_3)}{2(\delta_3+\gamma_3)-\gamma_1\delta_3}$$

$$\approxeq \frac{\sqrt{2\pi}\alpha_2^{1/4}e^{\Phi_-(z_-)/\sqrt{\alpha_2}}}{\sqrt{\frac{\gamma_1\delta_3}{c_0(\delta_3+\gamma_3)^{1/2}}\left(1-\frac{\delta_3+\gamma_3}{\gamma_1\delta_3}\right)}}. \tag{3.58}$$

Substituting this into our initial solution for u, Equation (3.29), we have

$$u(z;\alpha_2) \approxeq \sqrt{\frac{c_0\gamma_1\delta_3}{2\pi(\delta_3+\gamma_3)^{1/2}}\left(1-\frac{\delta_3+\gamma_3}{\gamma_1\delta_3}\right)}\alpha_2^{1/4}e^{(\Phi_-(z)-\Phi_-(z_-))/\sqrt{\alpha_2}} \tag{3.59}$$

and hence, at leading order,

(3.60)

$$u(z;\alpha_2) = \begin{cases} \sqrt{\frac{c_0\gamma_1\delta_3}{2\pi(\delta_3+\gamma_3)^{1/2}}\left(1-\frac{\delta_3+\gamma_3}{\gamma_1\delta_3}\right)}\alpha_2^{1/4}e^{(\Phi_-(z)-\Phi_-(z_-))/\sqrt{\alpha_2}} & \text{if } z<z_-, \\ 1-\frac{\gamma_1\delta_3}{\delta_3+\gamma_3}+\frac{\gamma_1\delta_3}{2(\delta_3+\gamma_3)}e^{\sqrt{\delta_3+\gamma_3}z} & \text{if } z_-<z<0, \\ 1-\frac{\gamma_1\delta_3}{2(\delta_3+\gamma_3)}e^{-\sqrt{\delta_3+\gamma_3}z} & \text{if } z>0. \end{cases}$$

In the inner region, letting $z=\sqrt{\alpha_2}\zeta$ gives

$$U(\zeta;\alpha_2) = u(\sqrt{\alpha_2}\zeta,\alpha_2) \approxeq \begin{cases} 1-\frac{\gamma_1\delta_3}{\delta_3+\gamma_3}+\frac{\gamma_1\delta_3}{2(\delta_3+\gamma_3)}e^{\sqrt{\delta_3+\gamma_3}\sqrt{\alpha_2}\zeta} & \text{if } \zeta<0, \\ 1-\frac{\gamma_1\delta_3}{2(\delta_3+\gamma_3)}e^{-\sqrt{\delta_3+\gamma_3}\sqrt{\alpha_2}\zeta} & \text{if } \zeta>0. \end{cases} \tag{3.61}$$

The leading order contribution is obtained by setting $\alpha_2=0$:

$$U_{in}(\zeta) = 1-\frac{\gamma_1\delta_3}{2(\delta_3+\gamma_3)} \quad \text{for any } \zeta \text{ in } \mathbb{R}.. \tag{3.62}$$

We discuss the relationship between the inner region solution in Case B and the possibility of an interstitial gap below, in conjunction with Case C.

Case C: $\frac{2(\delta_3+\gamma_3)}{\delta_3} < \gamma_1$

For $z>0$, if $z>z_+$, then for any $z\le s<\infty$ we have $s>z_+$ and

$$\Phi_+'(s) = \frac{1}{c_0}\left[\frac{\gamma_1\delta_3}{2(\delta_3+\gamma_3)}e^{-\sqrt{\delta_3+\gamma_3}s}-1\right] < \frac{1}{c_0}\left[\frac{\gamma_1\delta_3}{2(\delta_3+\gamma_3)}e^{-\sqrt{\delta_3+\gamma_3}z_+}-1\right] = 0. \tag{3.63}$$

Using Laplace's method,

$$\int_z^\infty e^{\Phi_+(s)/\sqrt{\alpha_2}}ds \approxeq -\frac{\sqrt{\alpha_2}e^{\Phi_+(z)/\sqrt{\alpha_2}}}{\Phi_+'(z)}, \tag{3.64}$$

so that our solution for u, Equation (3.29), when $z > z_+$ becomes

(3.65)
$$u \approxeq \frac{\sqrt{\alpha_2}c_0e^{\Phi_+(z)/\sqrt{\alpha_2}}}{\int_z^\infty e^{\Phi_+(s)/\sqrt{\alpha_2}}ds} = -\frac{\sqrt{\alpha_2}c_0e^{\Phi_+(z)/\sqrt{\alpha_2}}}{\sqrt{\alpha_2}e^{\Phi_+(z)/\sqrt{\alpha_2}}}\Phi_+'(z) = c_0\Phi_+'(z) = 1 - \frac{\gamma_1\delta_3}{2(\delta_3+\gamma_3)}e^{-\sqrt{\delta_3+\gamma_3}z}.$$

For $z > 0$, if $0 < z < z_+$, then using Laplace's method,

$$\int_z^\infty e^{\Phi_+(s)/\sqrt{\alpha_2}}ds \approxeq \frac{\sqrt{2\pi}\alpha_2^{1/4}e^{\Phi_+(z_+)/\sqrt{\alpha_2}}}{\sqrt{-\Phi_+''(z_+)}} = \sqrt{\frac{2\pi c_0}{\sqrt{\delta_3+\gamma_3}}}\alpha_2^{1/4}e^{\Phi_+(z_+)/\sqrt{\alpha_2}}. \tag{3.66}$$

So, from Equation (3.29), we find that if $0 < z < z_+$, then

$$u(z;\alpha_2) \approxeq \frac{\sqrt{\alpha_2}c_0e^{\Phi_+(z)/\sqrt{\alpha_2}}}{\int_z^\infty e^{\Phi_+(s)/\sqrt{\alpha_2}}ds} = \sqrt{\frac{c_0\sqrt{\delta_3+\gamma_3}}{2\pi}}\alpha_2^{1/4}e^{(\Phi_+(z)-\Phi_+(z_+))/\sqrt{\alpha_2}}. \tag{3.67}$$

For $z < 0$, again from Laplace's method,

$$\int_0^\infty e^{\Phi_+(s)/\sqrt{\alpha_2}}ds \approxeq \frac{\sqrt{2\pi}\alpha_2^{1/4}e^{\Phi_+(z_+)/\sqrt{\alpha_2}}}{\sqrt{-\Phi_+''(z_+)}} \approxeq \sqrt{\frac{2\pi c_0}{\sqrt{\delta_3+\gamma_3}}}\alpha_2^{1/4}e^{\Phi_+(z_+)/\sqrt{\alpha_2}}. \tag{3.68}$$

For any $z < s < 0$, we have

(3.69)
$$\Phi_-'(s) = \frac{1}{c_0}\left[\left(\frac{\gamma_1\delta_3}{\delta_3+\gamma_3}-1\right) - \frac{\gamma_1\delta_3}{2(\delta_3+\gamma_3)}e^{\sqrt{\delta_3+\gamma_3}s}\right] \geq \frac{1}{c_0}\left[\left(\frac{\gamma_1\delta_3}{\delta_3+\gamma_3}\right) - \frac{\gamma_1\delta_3}{2(\delta_3+\gamma_3)} - 1\right] > 0.$$

From Laplace's method,

$$\int_z^0 e^{\Phi_-(s)/\sqrt{\alpha_2}}ds \approxeq -\frac{\sqrt{\alpha_2}e^{\Phi_-(0)/\sqrt{\alpha_2}}}{\Phi_-'(0)} = \frac{2c_0\sqrt{\alpha_2}(\delta_3+\gamma_3)}{2(\delta_3+\gamma_3)-\gamma_1\delta_3}, \tag{3.70}$$

and

$$\int_z^0 e^{\Phi_-(s)/\sqrt{\alpha_2}}ds + \int_0^\infty e^{\Phi_+(s)\sqrt{\alpha_2}}ds \approxeq \frac{2c_0\sqrt{\alpha_2}(\delta_3+\gamma_3)}{2(\delta_3+\gamma_3)-\gamma_1\delta_3} + \sqrt{\frac{2\pi c_0}{\sqrt{\delta_3+\gamma_3}}}\alpha_2^{1/4}e^{\Phi_+(z_+)/\sqrt{\alpha_2}}$$

$$\approxeq \sqrt{\frac{2\pi c_0}{\sqrt{\delta_3+\gamma_3}}}\alpha_2^{1/4}e^{\Phi_+(z_+)/\sqrt{\alpha_2}} \tag{3.71}$$

since $\Phi_+(z_+) > 0$ and $\Phi_+(z_+)$ is independent of α_2. Thus, from Equation (3.29),

$$u(z;\alpha_2) \approxeq \sqrt{\frac{c_0\sqrt{\delta_3+\gamma_3}}{2\pi}}\alpha_2^{1/4}e^{(\Phi_-(z)-\Phi_+(z_+))/\sqrt{\alpha_2}} \qquad \text{if } z < 0. \tag{3.72}$$

Therefore, in the case that $\frac{2(\delta_3+\gamma_3)}{\delta_3} < \gamma_1$, the leading order solution for the outer region is

$$u(z;\alpha_2) \approxeq \begin{cases} \sqrt{\frac{c_0\sqrt{\delta_3+\gamma_3}}{2\pi}}\alpha_2^{1/4} e^{(\Phi_-(z)-\Phi_+(z_+))/\sqrt{\alpha_2}} & \text{if } z<0, \\ \sqrt{\frac{c_0\sqrt{\delta_3+\gamma_3}}{2\pi}}\alpha_2^{1/4} e^{(\Phi_+(z)-\Phi_+(z_+))/\sqrt{\alpha_2}} & \text{if } 0<z<z_+, \\ 1-\frac{\gamma_1\delta_3}{2(\delta_3+\gamma_3)}e^{-\sqrt{\delta_3+\gamma_3}z} & \text{if } z>z_+, \end{cases} \tag{3.73}$$

and for the inner region is

$$U(\zeta;\alpha_2) = u(\sqrt{\alpha_2}\zeta;\alpha_2) \approxeq \begin{cases} \sqrt{\frac{c_0\sqrt{\delta_3+\gamma_3}}{2\pi}}\alpha_2^{1/4} e^{(\Phi_-(\sqrt{\alpha_2}\zeta)-\Phi_+(z_+))/\sqrt{\alpha_2}} & \text{if } \zeta<0, \\ \sqrt{\frac{c_0\sqrt{\delta_3+\gamma_3}}{2\pi}}\alpha_2^{1/4} e^{(\Phi_+(\sqrt{\alpha_2}\zeta)-\Phi_+(z_+))/\sqrt{\alpha_2}} & \text{if } \zeta>0. \end{cases} \tag{3.74}$$

To explicitly calculate the inner solutions, we find

$$\begin{aligned} \frac{\Phi_-(\sqrt{\alpha_2}\zeta)}{\sqrt{\alpha_2}} &= \frac{1}{\sqrt{\alpha_2}c_0}\left[\frac{\gamma_1\delta_3}{2(\delta_3+\gamma_3)^{3/2}}\left(1-e^{\sqrt{\delta_3+\gamma_3}\sqrt{\alpha_2}\zeta}\right)-\sqrt{\alpha_2}\zeta\left(1-\frac{\gamma_1\delta_3}{\delta_3+\gamma_3}\right)\right] \\ &= \frac{\zeta}{c_0}\left[\frac{\gamma_1\delta_3}{2(\delta_3+\gamma_3)}-1\right]+O(\sqrt{\alpha_2}) \equiv \Phi_-^*, \end{aligned} \tag{3.75}$$

$$\begin{aligned} \frac{\Phi_+(\sqrt{\alpha_2}\zeta)}{\sqrt{\alpha_2}} &= \frac{1}{\sqrt{\alpha_2}c_0}\left[\frac{\gamma_1\delta_3}{2(\delta_3+\gamma_3)^{3/2}}\left(1-e^{-\sqrt{\delta_3+\gamma_3}\sqrt{\alpha_2}\zeta}\right)-\sqrt{\alpha_2}\zeta\right] \\ &= \frac{\zeta}{c_0}\left[\frac{\gamma_1\delta_3}{2(\delta_3+\gamma_3)}-1\right]+O(\sqrt{\alpha_2}) \equiv \Phi_+^*. \end{aligned} \tag{3.76}$$

With the above definitions, the fact that $\Phi_+(z_+) > 0$, and the restriction here that $1-\frac{\gamma_1\delta_3}{\delta_3+\gamma_3} < 0$,

$$\lim_{\alpha_2\to 0} U(\zeta;\alpha_2) = \begin{cases} \lim_{\alpha_2\to 0}\sqrt{\frac{c_0\sqrt{\delta_3+\gamma_3}}{2\pi}}\alpha_2^{1/4} e^{[\Phi_-^*-(\Phi_+(z_+)/\sqrt{\alpha_2})]} = 0 & \text{if } \zeta<0 \\ \lim_{\alpha_2\to 0}\sqrt{\frac{c_0\sqrt{\delta_3+\gamma_3}}{2\pi}}\alpha_2^{1/4} e^{[\Phi_+^*-(\Phi_+(z_+)/\sqrt{\alpha_2})]} = 0 & \text{if } \zeta>0. \end{cases} \tag{3.77}$$

Therefore, $U_{in}(\zeta) = 0$ for all ζ in $\mathbb{R}$. In summary, we have

$$U_{in}(\zeta) \approxeq \begin{cases} 1-\frac{\gamma_1\delta_3}{2(\delta_3+\gamma_3)} & \text{if } 0<\gamma_1<\frac{2(\delta_3+\gamma_3)}{\delta_3}, \\ 0 & \text{if } \gamma_1>\frac{2(\delta_3+\gamma_3)}{\delta_3}, \end{cases} \tag{3.78}$$

and thus from the analytical solution we see that an interstitial gap is present if $\gamma_1 > 2(\delta_3+\gamma_3)/\delta_3$. The presence of this gap was confirmed in numerical simulations (not shown).

Finally, we determine the minimal travelling wavespeed of the tumour density (v). Examining the inner solution

$$\left[\left(1-\frac{U_{in}}{1+K_*^{tis}}\right)V_{in}''-\frac{1}{1+K_*^{tis}}U_{in}'V_{in}'\right]+c_0V_{in}'+\delta_2V_{in}(1-V_{in})=0 \tag{3.79}$$

where $V_{in}(-\infty)=1$ and $V_{in}(\infty)=0$, if we define D_* such that

$$D_*=1-\frac{U_{in}}{1+K_*^{tis}}=\begin{cases}1-\dfrac{2(\delta_3+\gamma_3)-\gamma_1\delta_3}{2(\delta_3+\gamma_3)(1+K_*^{tis})} & \text{if } 0<\gamma_1<\frac{2(\delta_3+\gamma_3)}{\delta_3},\\ 1 & \text{if } \gamma_1>\frac{2(\delta_3+\gamma_3)}{\delta_3},\end{cases} \tag{3.80}$$

then the equation for V_{in} satisfies the Fisher-Kolmogorov equation

$$D_*V_{in}''+c_0V_{in}'+\delta_2V_{in}(1-V_{in})=0 \tag{3.81}$$

which is known to have a minimal wavespeed of $c_0\geq 2\sqrt{\delta_2D_*}$. As $c=c_0\sqrt{\alpha_2}$, the minimal wavespeed of Equation (3.81) is

$$c_{min}=\begin{cases}2\sqrt{\alpha_2\delta_2\left(1-\dfrac{2(\delta_3+\gamma_3)-\gamma_1\delta_3}{2(\delta_3+\gamma_3)(1+K_*^{tis})}\right)} & \text{if } 0<\gamma_1<\frac{2(\delta_3+\gamma_3)}{\delta_3},\\ 2\sqrt{\alpha_2\delta_2} & \text{if } \gamma_1>\frac{2(\delta_3+\gamma_3)}{\delta_3}.\end{cases} \tag{3.82}$$

We note that under conditions of no freedom of motility ($K_*^{tis}=0$) and no treatment ($\delta_3=0$), we recover the result found in [8]. Furthermore, a comparison of the analytically derived wavespeed with numerical simulations shows good agreement (Figure 3a). It is evident in Equation (3.82) that there exist parameter combinations such that for low tissue density (high K_*^{tis}) the magnitude of the treatment dose (γ_3) has no effect on wavespeed, but under higher tissue density, higher treatment dosing does reduce the wavespeed (Figure 3b). The former scenario replicates a primary tumour and the latter a metastatic tumour; therefore, our modelling verifies the possibility of tissue density as a consistent explanation for the difference in buffer efficacy between primary and metastatic tumours. However, it is important to note we do not base our parameter choices for K_* on experimentally derived values, due to a lack of availability in the current literature. Future work quantifying this parameter in different tissues would confirm the true magnitude of variability in K_*, and subsequent effect (if any) on invasion wavespeed.

We now move on to address our second experimentally-motivated question; that is, we consider the translational safety and efficacy of bicarbonate therapy in humans.

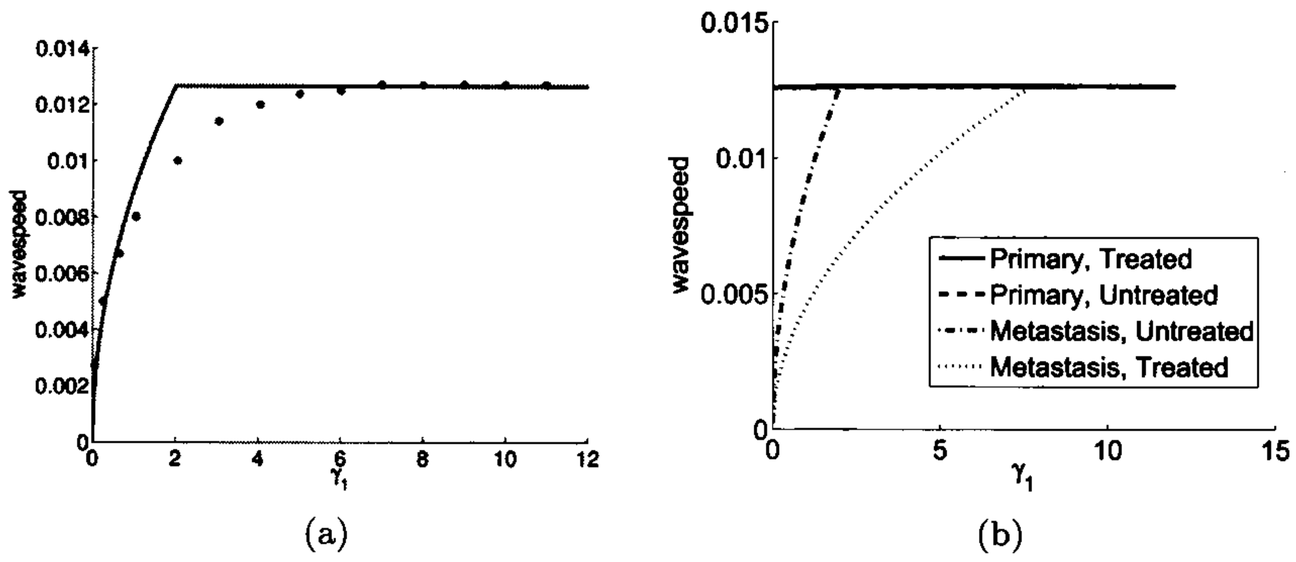

Figure 3: The analytical tumour wavespeed for varying values of the aggression parameter, γ_1. (a) A comparison of the analytical (line) and numerical (circles) wavespeeds. The analytical wavespeed is calculated from Equation (3.82), and the numerical wavespeed is calculated by solving Equations (3.1)-(3.3) using the Method of Lines and finite differences for a long time ($\tau = 20$) to ensure the decay of transients and that the waves are travelling at their asymptotic wavespeed. Here, $\delta_2 = 1$, $\alpha_2 = 4 \times 10^{-5}$, $\delta_3 = 70$, $K_* = 0$, $\gamma_3 = 0$, and γ_1 varies as dictated on the horizontal axis. There is good agreement for $\gamma_1 < 1$ and $\gamma_1 > 3$, and there is a small estimation error for $1 < \gamma_1 < 3$ due to the error introduced in the use of Laplace's method to approximate the normal tumour levels as used in this section. (b) The predicted effect of tissue density and treatment on the tumour invasion wavespeed, as found from the analytical wavespeed solution in Equation (3.82). The solid line is the wavespeed of untreated primary tumours on varying γ_1, and the dashed line is for treated primary tumours: these lines overlap as there is no difference in wavespeed for any value of γ_1. The dash-dot line is the wavespeed for untreated metastases, and the dotted line represents treated metastases. For all but very aggressive tumours (high values of γ_1), the treatment used slows the metastatic growth, but not the growth of the primary tumour. For the untreated metastasis, with $\gamma_1 <\approx 2$ such that there is contact between the tumour and the normal tissue, the wavespeed is slower than in primary tumours. For $\gamma_1 >\approx 2$, where a gap occurs at the tumour front, the wavespeed is independent of aggressivity. Note that a slowing of the primary tumour due to treatment could be found with the K_*^{tis} used in this figure, but only with very large treatment doses. Here parameters are $\gamma_1 = 0.5$, $\delta_2 = 1$, $\alpha_2 = 4 \times 10^{-5}$, $\delta_3 = 70$, $K_*^{primary} = 100$, $K_*^{metastasis} = 0$, and $\gamma_3 = 200, 0$ for treated and untreated cases, respectively. The system is solved with boundary and initial conditions as described in the text. The boundary and initial conditions are identical for all cases (primary, metastasis, treated, untreated).

§ 4. Translational safety and efficacy of bicarbonate therapy in humans

§ 4.1. A system of coupled nonlinear ordinary differential equations

Here we present a nonlinear ODE model of systemic buffering through the HCO_3^-/CO_2 buffering system, tracking extracellular pH (pHe) in the blood and tumour, and find a uniformly valid analytical approximation to the solution. We parameterise this model first for mice, comparing model predictions with experimental results, then re-parameterise for humans to generate predictions of bicarbonate safety and efficacy. Full details and a model derivation can be found in [6].

The first three equations capture the tumour dynamics, and will be discussed in turn below.

$$\frac{dB_t}{dt} = \overbrace{k_2C_t - k_1B_tH_t}^{\text{chemical reactions}} + \overbrace{g_1(B_b - B_t)}^{\text{vascular exchange}}, \tag{4.1}$$

$$\frac{dH_t}{dt} = \overbrace{k_2C_t - k_1B_tH_t}^{\text{chemical reactions}} + \overbrace{\phi_1}^{\text{tumour production}} - \overbrace{g_2(H_t - H_b)}^{\text{vascular exchange}}, \tag{4.2}$$

$$\frac{dC_t}{dt} = \overbrace{k_1B_tH_t - k_2C_t}^{\text{chemical reactions}} + \overbrace{\phi_5}^{\text{tumour production}} - \overbrace{g_3(C_t - C_b)}^{\text{vascular exchange}}. \tag{4.3}$$

The first two terms in each equation represent the bicarbonate buffering reaction kinetics in the tumour, and the final terms represent the vascular exchange between the blood and the tumour. Equation (4.1) describes the dynamics of tumour HCO_3^- (B_t). As there is no direct production or consumption of HCO_3^- in the tumour, this equation only includes chemical reaction terms and vascular exchange of HCO_3^-. Equation (4.2) models the tumour H^+ concentration (H_t). The third term, ϕ_1, is the net production of H^+ per unit volume of the tumour through aerobic glycolysis, implicitly incorporating the fixed contribution of minor additional non-motile tissue buffering components which act on a faster timescale than the other reactions detailed. This production term is generally higher than in normal tissue due to the upregulation of glycolysis in malignant tumours. Equation (4.3) represents the tumour CO_2 dynamics (C_t). The third term, ϕ_5, represents the tumour production of CO_2 from cellular metabolism.

The last three equations capture the blood dynamics,

$$\frac{dB_b}{dt} = \overbrace{k_2C_b - k_1B_bH_b}^{\text{chemical reactions}} + \overbrace{\phi_2C_b - \lambda_1B_b}^{\text{kidney filtration}} + \overbrace{\theta_1}^{\text{treatment}} - \overbrace{g_1v_T(B_b - B_t)}^{\text{vascular exchange}}, \tag{4.4}$$

$$\frac{dH_b}{dt} = \overbrace{k_2C_b - k_1B_bH_b}^{\text{chemical reactions}} + \overbrace{\phi_3}^{\text{body production}} + \overbrace{g_2v_T(H_t - H_b)}^{\text{vascular exchange}}, \tag{4.5}$$

$$\frac{dC_b}{dt} = \overbrace{k_1B_bH_b - k_2C_b}^{\text{chemical reactions}} + \overbrace{\phi_4}^{\text{body production}} - \overbrace{\lambda_2C_bf(C_b)}^{\text{ventilation}} + \overbrace{g_3v_T(C_t - C_b)}^{\text{vascular exchange}}. \tag{4.6}$$

As before, the first two terms in each equation represent the bicarbonate buffering reaction kinetics in the blood, and the final terms represent the vascular exchange between the blood and the tumour. Equation (4.4) describes the blood HCO_3^- (B_b), where the third and fourth terms are standard representations used to model the complex process of renal filtration and reabsorption of bicarbonate, with ϕ_2 as the acid secretion rate and λ_1 as the bicarbonate filtration rate. Further details of this system can be found in [6]. The fifth term, θ_1, is the bicarbonate treatment term. Equation (4.5) models the blood H^+ dynamics (H_b). The third term represents the net contribution of protons from the rest of the body tissues (except for the tumour) after the contribution of non-motile tissue buffers. Equation (4.6) models the blood CO_2 concentration (C_b). The third term is the CO_2 source from the normal body tissues; here ϕ_4 represents the rate of CO_2 entry into the bloodstream from the normal tissue. The fourth term in Equation (4.6) represents the regulation of blood CO_2 levels by respiration, where CO_2 lost through ventilation is proportional to the product of the ventilation rate, $f(C_b)$, and the CO_2 concentration. The function for ventilation we use is:

$$f(C_b) = \begin{cases} V_{min} & \text{if } f(C_b) < V_{min}, \\ V_{slope}C_b - V_{intercept} & \text{if } V_{min} < f(C_b) < V_{max}, \\ V_{max} & \text{if } f(C_b) > V_{max}. \end{cases} \tag{4.7}$$

The initial conditions are $C_b(0) = c_0$, $C_t(0) = c_0$, $B_b(0) = b_0$, $B_t(0) = b_0$, $H_b(0) = h_0$, and $H_t(0) = h_0$. We choose c_0, b_0, and h_0 to be the standard blood values of CO_2, HCO_3^-, and H^+, respectively.

In order to nondimensionalise our model, we use the rescaling $\tau = k_2 t$, $b_0 b_t = B_t$, $c_0 c_t = C_t$, $h_0 h_t = H_t$, $b_0 b_b = B_b$, $c_0 c_b = C_b$, and $h_0 h_b = H_b$ to obtain the system

$$\frac{db_t}{d\tau} = \delta_1(c_t - \alpha_2 b_t h_t) + \Gamma_1(b_b - b_t) \tag{4.8}$$

$$\frac{dh_t}{d\tau} = \delta_3(c_t - \alpha_2 b_t h_t) + \Phi_1 - \Gamma_2(h_t - h_b) \tag{4.9}$$

$$\frac{dc_t}{d\tau} = -(c_t - \alpha_2 b_t h_t) + \Phi_5 - \Gamma_3(c_t - c_b) \tag{4.10}$$

$$\frac{db_b}{d\tau} = \delta_1(c_b - \alpha_2 b_b h_b) + \Phi_2 c_b - \xi_1 b_b + \Theta_1 - \Gamma_1 v_T(b_b - b_t) \tag{4.11}$$

$$\frac{dh_b}{d\tau} = \delta_3(c_b - \alpha_2 b_b h_b) + \Phi_3 + \Gamma_2 v_T(h_t - h_b) \tag{4.12}$$

$$\frac{dc_b}{d\tau} = -(c_b - \alpha_2 b_b h_b) + \Phi_4 - \xi_3(c_b)c_b + \Gamma_3 v_T(c_t - c_b). \tag{4.13}$$

The ventilation function is

$$\xi_3(c_b) = \begin{cases} \Delta_{min} & \text{if } \xi_3(c_b) < \Delta_{min}, \\ \Delta_1 c_b - \Delta_2 & \text{if } \Delta_{min} < \xi_3(c_b) < \Delta_{max}, \\ \Delta_{max} & \text{if } \xi_3(c_b) > \Delta_{max}, \end{cases} \tag{4.14}$$

where $\Delta_{min} = \frac{\lambda_2}{k_2} V_{min}$, $\Delta_1 = \frac{\lambda_2}{k_2} V_{slope} c_0$, $\Delta_2 = \frac{\lambda_2}{k_2} V_{intercept}$, and $\Delta_{max} = \frac{\lambda_2}{k_2} V_{max}$, and the initial conditions are

$$c_b(0) = 1,\ c_t(0) = 1,\ b_b(0) = 1,\ b_t(0) = 1,\ h_b(0) = 1,\ \text{and } h_t(0) = 1. \tag{4.15}$$

The nondimensional parameters are given in Table 1.

Name	Mouse	Human
δ_1	5.0×10^{-2}	5.0×10^{-2}
Γ_1	2.5×10^{-8}	2.5×10^{-8}
δ_3	3.02×10^{4}	3.02×10^{4}
Φ_1	7.17×10^{-3}	7.17×10^{-3}
Γ_2	8.79×10^{-8}	8.79×10^{-8}
α_2	1.0	1.0
Φ_5	6.11×10^{-9}	7.63×10^{-9}
Γ_3	7.32×10^{-7}	7.32×10^{-7}
Φ_2	1.13×10^{-7}	2.11×10^{-8}
ξ_1	1.10×10^{-7}	1.90×10^{-8}
Θ_1	1.16×10^{-8}	9.16×10^{-10}
$v_T\Gamma_1$	2.5×10^{-9}	2.5×10^{-10}
Φ_3	1.28×10^{-3}	1.1×10^{-3}
$v_T\Gamma_2$	8.79×10^{-9}	8.79×10^{-10}
Φ_4	1.13×10^{-6}	9.16×10^{-8}
$v_T\Gamma_3$	7.32×10^{-8}	7.32×10^{-9}
Δ_{min}	5.23×10^{-7}	3.08×10^{-8}
Δ_1	1.52×10^{-6}	2.03×10^{-6}
Δ_2	3.51×10^{-7}	1.9×10^{-6}
Δ_{max}	2.05×10^{-6}	1.54×10^{-6}

Table 1: Mouse and human nondimensionalised parameter values. Parameter derivation and references can be found in [6].

§ 4.2. Nonstandard asymptotics for three characteristic timescales

Many models of biological systems incorporate multiple characteristic timescales, generally indicated by parameters that span several orders of magnitude. In our system, important processes include chemical reaction dynamics on the order of nano- to milliseconds, cellular production of protons on the order of seconds (Φ_1 and Φ_3), and physiological processes, such as ventilation and kidney filtration, on the order of minutes to hours (Φ_2, Δ_1, Δ_2). Standard asymptotic analysis is inadequate for such a system; instead, it is possible to employ selective rescalings to find approximate solutions within each timescale separately. We separate timescales into those associated with ultrafast reaction dynamics, fast cellular processes, and slow physiological processes by using the scaled variables $\tau, \tau_2 = \epsilon\tau, \tau_3 = \epsilon^2\tau$ with $\epsilon = 10^{-3}$. All parameters except δ_1, δ_3, and α_2 are then written in terms of powers of ϵ with order unity coefficients to enable a multiscale analysis at each of the appropriate timescales before the construction of a uniform, asymptotically accurate, solution. The parameters δ_1, δ_3, and α_2 are not written in powers of ϵ as they control the chemical reaction dynamics on the fast timescale, and thus do not need to be separated at a higher resolution for the approximation of the solution.

The system dynamics on the fast timescale are dominated by chemical reactions (on the order of nano- to milli-seconds). Accordingly, we define $\epsilon = 10^{-3}$, and rescale Equations (4.8)-(4.13) to

$$\frac{db_t}{d\tau} = \delta_1(c_t - \alpha_2 b_t h_t) + \epsilon^2\hat{\Gamma}_1(b_b - b_t) \tag{4.16}$$

$$\frac{dh_t}{d\tau} = \delta_3(c_t - \alpha_2 b_t h_t) + \epsilon\hat{\Phi}_1 - \epsilon^2\hat{\Gamma}_2(h_t - h_b) \tag{4.17}$$

$$\frac{dc_t}{d\tau} = -(c_t - \alpha_2 b_t h_t) + \epsilon^2\hat{\Phi}_5 - \epsilon^2\hat{\Gamma}_3(c_t - c_b) \tag{4.18}$$

$$\frac{db_b}{d\tau} = \delta_1(c_b - \alpha_2 b_b h_b) + \epsilon^2\hat{\Phi}_2 c_b - \epsilon^2\hat{\xi}_1 b_b + \epsilon^2\hat{\Theta}_1 - \epsilon^2\hat{\Gamma}_1 v_T(b_b - b_t) \tag{4.19}$$

$$\frac{dh_b}{d\tau} = \delta_3(c_b - \alpha_2 b_b h_b) + \epsilon\hat{\Phi}_3 + \epsilon^2\hat{\Gamma}_2 v_T(h_t - h_b) \tag{4.20}$$

$$\frac{dc_b}{d\tau} = -(c_b - \alpha_2 b_b h_b) + \epsilon^2\hat{\Phi}_4 - \epsilon^2\hat{\xi}_3(c_b)c_b + \epsilon^2\hat{\Gamma}_3 v_T(c_t - c_b), \tag{4.21}$$

where $\delta_1 = \frac{c_0}{b_0}$, $\alpha_2 = \frac{k_1 h_0 b_0}{k_2 c_0}$, $\hat{\Gamma}_1 = \frac{g_1}{\epsilon^2 k_2}$, $\delta_3 = \frac{c_0}{h_0}$, $\hat{\Phi}_1 = \frac{\phi_1}{\epsilon k_2 h_0}$, $\hat{\Gamma}_2 = \frac{g_2}{\epsilon^2 k_2}$, $\hat{\Gamma}_3 = \frac{g_3}{\epsilon^2 k_2}$, $\hat{\Phi}_2 = \frac{\phi_2 c_0}{\epsilon^2 k_2 b_0}$, $\hat{\xi}_1 = \frac{\lambda_1}{\epsilon^2 k_2}$, $\hat{\Theta}_1 = \frac{\theta_1}{\epsilon^2 k_2 b_0}$, $\hat{\Phi}_3 = \frac{\phi_3}{\epsilon k_2 h_0}$, $\hat{\Phi}_4 = \frac{\phi_4}{\epsilon^2 k_2 c_0}$, $\hat{\xi}_3(c_b) = \frac{\lambda_2}{\epsilon^2 k_2} f(c_b)$.

The ventilation function becomes

$$\hat{\xi}_3(c_b) = \begin{cases} \hat{\Delta}_{min} & \text{if } \xi_3(c_b) < \hat{\Delta}_{min}, \\ \hat{\Delta}_1 c_b - \hat{\Delta}_2 & \text{if } \hat{\Delta}_{min} < \hat{\xi}_3(c_b) < \hat{\Delta}_{max}, \\ \hat{\Delta}_{max} & \text{if } \hat{\xi}_3(c_b) > \hat{\Delta}_{max}, \end{cases} \tag{4.22}$$

with $\hat{\Delta}_{min} = \frac{\lambda_2}{\epsilon^2 k_2} V_{min}$, $\hat{\Delta}_1 = \frac{\lambda_2}{\epsilon^2 k_2} V_{slope} c_0$, $\hat{\Delta}_2 = \frac{\lambda_2}{\epsilon^2 k_2} V_{intercept}$, and $\hat{\Delta}_{max} = \frac{\lambda_2}{\epsilon^2 k_2} V_{max}$.

The reaction dynamics can be decoupled via the substitutions $u_1 = b_t + \delta_1 c_t$, $u_2 = b_b + \delta_1 c_b$, $v_1 = h_t + \delta_3 c_t$, $v_2 = h_b + \delta_3 c_b$. This does not scale the variables $v_{1,2}$ to O(1), but to O(δ_3)=O(10^4); however, the advantage is that the leading order equations simplify on noting the size of $v_{1,2}$, yielding

$$\frac{du_1}{d\tau} = \frac{dv_1}{d\tau} = 0 \tag{4.23}$$

$$\frac{dh_t}{d\tau} = v_1 - h_t - \alpha_2 h_t(\delta_3 u_1 - \delta_1 v_1 + \delta_1 h_t) \tag{4.24}$$

$$\frac{du_2}{d\tau} = \frac{dv_2}{d\tau} = 0 \tag{4.25}$$

$$\frac{dh_b}{d\tau} = v_2 - h_b - \alpha_2 h_b(\delta_3 u_2 - \delta_1 v_2 + \delta_1 h_b). \tag{4.26}$$

It is clear that u_1, v_1, u_2 and v_2 are constants, denoted A_1, A_2, A_3, and A_4, respectively; hence

$$\frac{dh_t}{d\tau} = -\alpha_2 \delta_1 h_t^2 + (-1 - \delta_3 \alpha_2 A_1 + \delta_1 \alpha_2 A_2) h_t + A_2 \tag{4.27}$$

$$\frac{dh_b}{d\tau} = -\alpha_2 \delta_1 h_b^2 + (-1 - \delta_3 \alpha_2 A_3 + \delta_1 \alpha_2 A_4) h_b + A_4. \tag{4.28}$$

These equations have one positive, stable steady state given by the appropriate roots, which we denote $\tilde{h}_{t+}$ and $\tilde{h}_{b+}$, of the quadratic right-hand side. Therefore, the solution in our original variables, denoted W_{fast}, satisfies (4.27), (4.28), and

$$c_t = \frac{1}{\delta_3}(A_2 - h_t) \quad c_b = \frac{1}{\delta_3}(A_4 - h_b) \tag{4.29}$$

$$b_t = A_1 - \frac{\delta_1}{\delta_3} A_2 + \frac{\delta_1}{\delta_3} h_t \quad b_b = A_3 - \frac{\delta_1}{\delta_3} A_4 + \frac{\delta_1}{\delta_3} h_b \tag{4.30}$$

where A_1, A_2, A_3, A_4 can be written in terms of the initial conditions. A comparison between the numerical and analytical solutions for the fast timescale shows good agreement for both tumour (Figure 4a) and blood (not shown).

To examine the intermediate timescale dynamics, we rescale time such that $\tau_2 = \epsilon\tau$. Noting again that our variables $v_{1,2}$ are not scaled to O(1) but to O(δ_3)=O(10^4), we

have at leading order:

$$\frac{du_1}{d\tau_2} = 0 \tag{4.31}$$

$$\frac{dv_1}{d\tau_2} = \hat{\Phi}_1 + \delta_3\epsilon\hat{\Phi}_5 - \epsilon\hat{\Gamma}_3(v_1 - v_2) \tag{4.32}$$

$$0 = -\alpha_2\delta_1 h_t^2 + (-1 - \delta_3\alpha_2 u_1 + \delta_1\alpha_2 v_1)h_t + v_1 \tag{4.33}$$

$$\frac{du_2}{d\tau_2} = 0 \tag{4.34}$$

$$\frac{dv_2}{d\tau_2} = \hat{\Phi}_3 + \delta_3\epsilon\hat{\Phi}_4 - \epsilon\left(\frac{\hat{\Delta}_1}{\delta_3}v_2^2 - \hat{\Delta}_2 v_2\right) + \epsilon\hat{\Gamma}_3 v_T(v_1 - v_2) \tag{4.35}$$

$$0 = -\alpha_2\delta_1 h_b^2 + (-1 - \delta_3\alpha_2 u_2 + \delta_1\alpha_2 v_2)h_b + v_2. \tag{4.36}$$

We see immediately that, as previously, u_1 and u_2 are constant and are denoted by A_1 and A_3, respectively, which can be written in terms of the initial conditions. Furthermore, h_t and h_b have reached their slow dynamics steady states, $\tilde{h}_{t+}$ and $\tilde{h}_{b+}$, and we are left with only Equations (4.32) and (4.35), where the initial conditions for v_1 and v_2 are the equilibrium values from the fast dynamics. These in turn are the parameters A_2 and A_4 and can be written in terms of the full model initial conditions. The positive equilibrium solutions, which we denote by $\tilde{v}_1$ and $\tilde{v}_2$, are linearly stable by standard linear analysis.

Transforming back into the original variables, the solutions, denoted $W_{intermediate}$, satisfy Equations (4.27) and (4.28) with h_t and h_b constant and

$$c_t = \frac{1}{\delta_3}(v_1 - h_t), \quad c_b = \frac{1}{\delta_3}(v_2 - h_b), \tag{4.37}$$

$$b_t = A_1 - \frac{\delta_1}{\delta_3}(v_1 - h_t), \quad b_b = A_3 - \frac{\delta_1}{\delta_3}(v_2 - h_b). \tag{4.38}$$

A comparison betwen the numerical and analytical solutions for the intermediate timescale shows good agreement for both tumour (Figure 4b) and blood (not shown).

Finally, the slow timescale is dominated by high-level physiological responses, such as ventilation and kidney excretion. Rescaling in time such that $\tau_3 = \epsilon^2\tau$, we note once again that $v_{1,2} \sim O(\delta_3) = O(10^4)$ and hence we consider each term in turn when

approximating to leading order. Thus we have

$$\frac{du_1}{d\tau_3} = \hat{\Gamma}_1\left(u_2 - \frac{\delta_1}{\delta_3}v_2 - u_1 + \frac{\delta_1}{\delta_3}v_1\right) + \delta_1\hat{\Phi}_5 - \hat{\Gamma}_3\frac{\delta_1}{\delta_3}(v_1 - v_2) \tag{4.39}$$

$$0 = \hat{\Phi}_1 + \delta_3\epsilon\hat{\Phi}_5 - \epsilon\hat{\Gamma}_3(v_1 - v_2) \tag{4.40}$$

$$0 = -\alpha_2\delta_1 h_t^2 + (-1 - \delta_3\alpha_2 u_1 + \delta_1\alpha_2 v_1)h_t + v_1 \tag{4.41}$$

$$\frac{du_2}{d\tau_3} = \frac{\hat{\Phi}_2}{\delta_3}v_2 - \hat{\xi}_1\left(u_2 - \frac{\delta_1}{\delta_3}v_2\right) + \hat{\Theta}_1 - \hat{\Gamma}_1 v_T\left(u_2 - \frac{\delta_1}{\delta_3}v_2 - u_1 + \frac{\delta_1}{\delta_3}v_1\right)$$

$$+ \delta_1\hat{\Phi}_4 - \frac{\delta_1\hat{\Delta}_1}{\delta_3^2}v_2^2 + \frac{\delta_1\hat{\Delta}_2}{\delta_3}v_2 + \hat{\Gamma}_3 v_T\frac{\delta_1}{\delta_3}(v_1 - v_2) \tag{4.42}$$

$$0 = \hat{\Phi}_3 + \delta_3\epsilon\hat{\Phi}_4 - \epsilon\left(\frac{\hat{\Delta}_1}{\delta_3}v_2^2 - \hat{\Delta}_2 v_2\right) + \epsilon\hat{\Gamma}_3 v_T(v_1 - v_2) \tag{4.43}$$

$$0 = -\alpha_2\delta_1 h_b^2 + (-1 - \delta_3\alpha_2 u_2 + \delta_1\alpha_2 v_2)h_b + v_2. \tag{4.44}$$

The initial conditions are the intermediate timescale equilibrium values for $u_{1,2}$ (denoted A_1 and A_3, respectively), which are ultimately derived from the initial conditions of the full model. For our parameters, the equilibrium values are positive, denoted $\tilde{u_1}$ and $\tilde{u_2}$, and comprise a linearly stable node. Transforming back into our original variables, the slow solution, W_{slow}, satisfies

$$c_t = \frac{1}{\delta_3}(v_1 - h_t), \quad c_b = \frac{1}{\delta_3}(v_2 - h_b) \tag{4.45}$$

$$b_t = u_1 - \frac{\delta_1}{\delta_3}(v_1 - h_t), \quad b_b = u_2 - \frac{\delta_1}{\delta_3}(v_2 - h_b). \tag{4.46}$$

Explicit large time asymptotic solutions are found readily and yield the steady state solutions in our original variables. By extracting leading order terms with our chosen parameters, we find

$$\tilde{h}_t = \frac{\left(\frac{\delta_3\hat{\Delta}_2}{\hat{\Delta}_1} + \frac{\hat{\Phi}_1}{\epsilon\hat{\Gamma}_3}\right)}{\delta_3\alpha_2\left(\frac{\hat{\Phi}_2\hat{\Delta}_2}{\hat{\xi}_1\hat{\Delta}_1} - \frac{\delta_1\hat{\Phi}_1}{\hat{\Gamma}_1\delta_3\epsilon}\right)} + O\left(\frac{1}{\delta_3}\right). \tag{4.47}$$

To leading order $\tilde{h}_t$ is proportional to $\hat{\xi}_1$ and inversely proportional to α_2, $\hat{\Gamma}_3$, $\hat{\Gamma}_1$, and $\hat{\Phi}_2$, so that H^+ levels in the tumour can be lowered either by decreasing the glomerular filtration rate (ξ_1) or by increasing the acid secretion rate (Φ_2), carbon dioxide vessel permeability (Γ_3), or bicarbonate vessel permeability (Γ_1). A comparison between the numerical and analytical solutions for the slow timescale shows good agreement for both tumour (Figure 4b) and blood (not shown).

It is now straightforward to construct an approximate uniformly valid solution using our fast, intermediate, and slow solutions. This uniform solution has the form

$$W_{uniform} = W_{fast} + W_{intermediate} + W_{slow} - \tilde{W}_{fast} - \tilde{W}_{intermediate} \tag{4.48}$$

where $\tilde{W}_{fast,intermediate}$ are the quasi-steady state solutions to the W_{fast} and $W_{intermediate}$ equations, respectively. These results are in good agreement with numerics [6].

Two conclusions have arisen from this analysis. First, a dangerous rise in blood pH is predicted in mice at the established dosage levels; this rise has been confirmed experimentally [6]. Second, re-parameterisation of the model suggests that bicarbonate therapy will have a reduced efficacy in humans. Our derived, uniformly valid, solutions are amenable to a sensitivity analysis that can suggest possible methods for increasing efficacy; these include alternative buffers and combination therapies that target aspects of renal function in conjunction with bicarbonate. Further details can be found in [6].

§ 5. Discussion

We have presented a system of coupled nonlinear PDEs to describe acid-mediated invasion, focusing on the dynamics of invasion that occur after destabilisation of the healthy steady state by the developing tumour, and have dealt to asymptotic accuracy with the subtleties of the resulting invasive tumour wavefront. We also have addressed the question of buffer efficacy in humans by deriving an ODE model and utilising a nonstandard scaling to clarify, again to asymptotic accuracy, the behaviour across three timescales of biological interest. Together these models and analyses have yielded valuable insights into tumour-host behaviour and therapeutic possibilities, and motivate further experiments, such as additional mouse studies in which tumours are implanted in different types of tissue to further elucidate the role of tissue density in acid-mediated invasion. In the case of the first model, however, several mathematical questions remain. Our asymptotics have confirmed that although the system is more complicated and in a higher dimension than the canonical Fisher-Kolmogorov system, it does appear to evolve to the minimum wavespeed; but as asymptotic techniques are not rigorous, the existence of this minimum wavespeed remains an open question. Further complications arise from propagation into an unstable steady state, including uncertainty of velocity selection due to degeneracy of the dynamics [9, 10], and robustness to fluctuations, a topic important to mathematical biology in general. These are ongoing mathematical problems and can be explored using (for example) the concept of marginal stability [11].

Additionally, underlying simplifying assumptions render the models presented here incomplete descriptions of acid-mediated invasion. For example, they omit competition between tumour and healthy cells for space and resources, justified in [5] by restricting the scope to cases in which the tumour and host populations are sharply delineated; but this limits the flexibility for accommodating microenvironmental complexity and clinical variation in tumour aggressiveness. In fact, adding cellular competition to the model [5] can produce, under low-acid conditions, tumours that establish standing rather than invading waves. As these are stable to perturbations they may represent benign tumours,

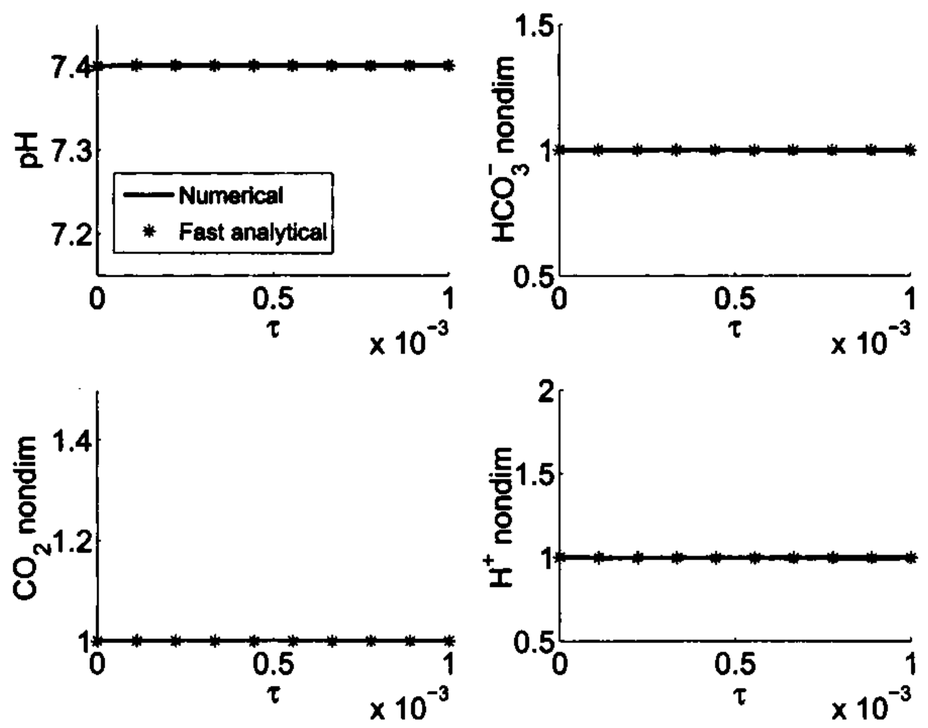

(a)

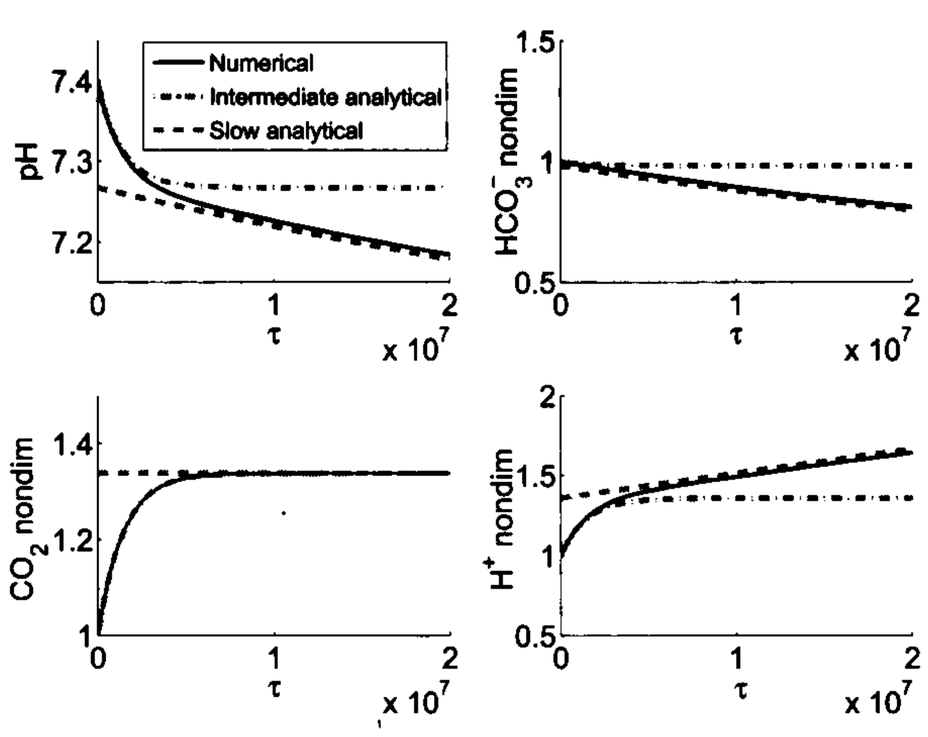

(b)

Figure 4: Comparison of numerical (stars) and approximate analytical solutions (lines) in the tumour for the (a) fast and (b) intermediate and slow timescales in an untreated human. In both (a) and (b), shown are the pH (upper left) and nondimensional HCO_3^- (upper right), CO_2 (lower left), and H^+ (lower right) over appropriately scaled time. The analytical solutions for the intermediate and slow timescales are calculated with initial conditions as the steady-state solutions of the fast and intermediate timescales, respectively. Both numerical and analytical solutions were calculated with the human parameters as in Table 1, but with $\Theta_1 = 0$.

and thus potentially are important features which have been explored recently (McGillen et al., in preparation). In general, for a full picture of a developing tumour it is necessary to determine how the tissue-level properties of invasion emerge from the underlying behaviour of individual cells at the tumour-host interface, and therefore continuum modelling alone is insufficient for a truly comprehensive understanding. Instead, a dual approach is needed in which the strengths of each approach compensate for weaknesses in the other. Population-level continuum models, such as those presented herein, are mathematically tractable but less accurate, while discrete stochastic representations, such as hybrid cellular automata approaches [12], capture fine detail but the formulation and large parameter sets preclude rigorous mathematical analysis. Thus, there is great scope for developing both in parallel so that, in the long term, we can make strides toward the realisation of therapies that contain and reduce the threat of cancer.

Acknowledgments

PKM was partially supported by a Royal Society Wolfson Research Merit award. JBM, NKM, and PKM were partially supported by the National Cancer Institute, NIH grant U54CA143970. NKM and PKM were partially supported by the National Cancer Institute, NIH grant U56CA113004. IR was supported by NIH grant R01CA077575.

References

[1] Cairns R, Harris I, and Mak T. Regulation of cancer cell metabolism. *Nature Reviews Cancer*, 11:85–95, 2011.

[2] Gatenby RA, Gawlinski ET, Gmitro AF, Kaylor B, and Gillies RJ. Acid-mediated tumor invasion: a multidisciplinary study. *Cancer Research*, 66(10):5216–5223, 2006.

[3] Warburg O. *The Metabolism of Tumors*. Arnold Constable, London, 1930.

[4] Gatenby RA and Maini PK. Mathematical oncology: cancer summed up. *Nature*, 421(6921):321, 2003.

[5] Gatenby RA and Gawlinski ET. A reaction-diffusion model of cancer invasion. *Cancer Research*, 56(24):5745–5753, 1996.

[6] Martin NK, Gaffney EA, Gatenby RA, Gillies RJ, Robey IF, and Maini PK. A mathematical model of tumour and blood pHe regulation: The HCO3-/CO2 buffering system. *Mathematical Biosciences*, 230:1–11, 2011.

[7] Robey IF, Baggett BK, Kirkpatrick ND, Roe DJ, Dosescu J, Sloane BF, Hashim AI, Morse DL, Raghunand N, Gatenby RA, and Gillies RJ. Bicarbonate increases tumor pH and inhibits spontaneous metastases. *Cancer Research*, 69:2260–8, 2009.

[8] Fasano A, Herrero MA, and Rodrigo MR. Slow and fast invasion waves in a model of acid-mediated tumour growth. *Mathematical Biosciences*, 220(1):45–56, 2009.

[9] Kessler DA, Ner Z, and Sander LM. Front propagation: precursors, cutoffs, and structural stability. *Physical Review E*, 58(1):107–114, 1998.

[10] Panja D. Effects of fluctuations on propagating fronts. *Physical Reports*, 393:87–174, 2004.

[11] Saarloos W. Front propagation into unstable states: marginal stability as a dynamical mechanism for velocity selection. *Physical Review A*, 37(1):211–229, 1988.

[12] Smallbone K, Gatenby RA, Gillies RJ, Maini PK, and Gavaghan D. Metabolic changes during carcinogenesis: potential impact on invasiveness. *Journal of Theoretical Biology*, 244(4):703–713, 2007.